Electronic structure and charge transport in nonstoichiometric tantalum oxide

T V Perevalov[1,2] , **V A Gritsenko**[1,2,3] , **A A Gismatulin**[1] ,
V A Voronkovskii[1] , **A K Gerasimova**[1] , **V Sh Aliev**[1] **and I A Prosvirin**[4]

[1] Rzhanov Institute of Semiconductor Physics SB RAS, 13 Lavrentiev Ave., 630090, Novosibirsk, Russia
[2] Novosibirsk State University, 2 Pirogov Str., 630090, Novosibirsk, Russia
[3] Novosibirsk State Technical University, 20 Marks ave., 630073, Novosibirsk, Russia
[4] Boreskov Institute of Catalysis SB RAS, 5 Lavrentiev ave., 630090, Novosibirsk, Russia

E-mail: timson@isp.nsc.ru

CrossMark

Abstract

The atomic and electronic structure of nonstoichiometric oxygen-deficient tantalum oxide $TaO_{x<2.5}$ grown by ion beam sputtering deposition was studied. The TaO_x film content was analyzed by x-ray photoelectron spectroscopy and by quantum-chemistry simulation. TaO_x is composed of Ta_2O_5, metallic tantalum clusters and tantalum suboxides. A method for evaluating the stoichiometry parameter of TaO_x from the comparison of experimental and theoretical photoelectron valence band spectra is proposed. The charge transport properties of TaO_x were experimentally studied and the transport mechanism was quantitatively analyzed with four theoretical dielectric conductivity models. It was found that the charge transport in almost stoichiometric and nonstoichiometric tantalum oxide can be consistently described by the phonon-assisted tunneling between traps.

Keywords: electronic structure, oxygen vacancy, photoelectron spectroscopy, quantum-chemistry calculations, charge localization, charge transport

(Some figures may appear in colour only in the online journal)

1. Introduction

Ta_2O_5 films have a high dielectric permittivity in the range of 20–50 and they are used as an insulator in dynamic random-access memories (DRAM) [1–4]. In addition, Ta_2O_5 films are used as a storage medium instead of silicon nitride in flash memory elements [5]. Nonstoichiometric $TaO_{x<2.5}$ films are used as a storage medium in a new generation of fast-acting nonvolatile resistive random-access memories (ReRAM) [6–14]. ReRAM is considered both for stand-alone data storage applications and as an embedded non-volatile memory. Among various oxide-based resistive switching elements, TaO_x-based devices exhibit excellent endurance (number of switching cycles) [6], memory retention performance [13], switching speed [14], and low power consumption [7]. The change in the TaO_x stoichiometry leads to a change in its electronic structure, and knowledge of the subtleties of this

process opens the possibility of controlling electrical properties.

The leakage current is one of the most important properties of dielectric films in any solid-state electronic device. The leakage current magnitude for a given electric field and temperature is determined by the charge transport mechanism [15]. The tantalum oxide-based ReRAM is operating on resistance changes of oxide layer in the metal-insulator-metal (MIM) structure, as is commonly believed, due to forming and disruption of a conducting filament, i.e. high metal-enrichment local region TaO_x. Despite a large number of contributions focused on charge transport in high resistance state (HRS) and low resistance state (LRS) of tantalum oxide-based ReRAM memories [11, 16, 17], there are only a limited number of studies of the nonstoichiometric tantalum oxide conduction mechanisms before the forming process and their connection with traps. The actual conduction model of TaO_x

before the filament forming is important for understanding of the nature of the forming in ReRAM structures.

Trap ionization via the Frenkel mechanism is often proposed to describe the charge transport in Ta_2O_5 [18–20]. However, the preexponential fitting factor is not analyzed in those studies, while it can be one of the criteria of the Frenkel model applicability. It is the nonphysical low value of the preexponential fitting factor that facilitated establishing that the Frenkel model is not suitable to describe the charge transport in Si_3N_4 and HfO_2 [21, 22]. Thus, the charge transport mechanism of tantalum oxide films is a matter that requires a detailed investigation. In [23] the charge transport in Ta_2O_5 is described in the framework of the numerical model of trap-assisted tunneling of electrons through traps. However, this complicated model makes a strong assumption that there is a continuous spectrum of the defect density of states in the bandgap, and the shape of this spectrum is not defined. Recently it was shown that tantalum oxide conductivity can be described within the phonon-assisted tunneling between traps model [24]. Notwithstanding that, other possible conduction mechanisms were not considered.

Thus, though the charge transport in metal-enriched TaO_x was investigated previously, the details of the process and connection with high concentrations of oxygen vacancies were not established. At the same time, understanding the charge transport mechanism in TaO_x films and its connection with electronic properties is important for the device operation and prediction of ReRAM reliability. The purpose of the current work is the investigation of the electronic structure and the revealing of the conductivity mechanism of nonstoichiometric tantalum oxide.

2. Materials and methods

Two groups of samples were prepared for this study. The first group consisted of the samples used for electron microscopy and photoelectron spectroscopy, which were fabricated as follows. Si (100) substrates with a resistivity of $4.5\ \Omega \cdot cm$ underwent cleaning by HF etching. Then TaO_x films were deposited by ion-beam sputtering deposition (IBSD) on these substrates. During this process, the Ta target was sputtered by the beam of Ar^+ ions and, simultaneously, high-purity oxygen ($O_2 > 99.999\%$) was introduced in the depositing chamber. The oxygen partial pressure $P(O_2)$ was varied by the gas flow controller for different samples, which allowed us to obtain tantalum oxide films with differing [O]/[Ta] ratios (x), varying from almost a stoichiometric composition ($x \approx 5/2$) to nonstoichiometric types ($x < 5/2$), as presented in table 1. The TaO_x film thicknesses were about 50 nm. The second group of samples, used for charge transport studies, represented $TaN/TaO_x(30\ nm)/Ni$ MIM structures on Si/SiO_2 substrates (see figure 1(a)) with the TaO_x layer being deposited in a manner similar to that described above for the first group of samples. The TaO_x layers for MIM structures were synthesized by IBSD at 9.34 mPa, 6.05 mPa, 3.91 mPa, 3.27 mPa and 2.66 mPa oxygen partial pressures.

Table 1. The used oxygen partial pressure in the depositing chamber, phase composition of TaO_x and the atomic ratio [O]/[Ta] obtained from the integral XPS peak intensities and of core levels from the comparison of experimental and theoretical VB XPS.

sample #	$P(O_2)$, 10^{-3} Pa	TaO_x phase composition, % at.			[O]/[Ta], from XPS	[O]/[Ta], from DFT
		Ta $_{met.}$	TaO_y	Ta_2O_5		
S1	9.09	0	0	100	2.77	2.50
S2	3.49	0	0	100	2.79	2.48
S3	2.81	5.8	10.3	83.8	2.59	2.42
S4	2.21	5.9	13.9	80.2	2.44	2.31
S5	1.71	6.7	18.3	74.9	2.22	2.19
S6	1.35	14.0	15.8	70.3	2.13	2.13
S7	1.08	18.3	19.6	62.1	1.99	2.00
S8	0.53	27.5	6.6	65.9	1.94	1.88

The surface morphology of TaO_x films was studied by field emission scanning electron microscopy (FESEM) using a Zeiss 1540 crossbeam system. The x-ray photoelectron spectra (XPS) were recorded on a SPECS (Germany) photoelectron spectrometer using a hemispherical PHOIBOS-150-MCD-9 analyzer and FOCUS-500 (Al K_α radiation, hν = 1486.74 eV, 200 W) monochromator. The peak binding energy (BE) was calibrated by the position of the C1s peak (BE = 284.8 eV) corresponding to the surface hydrocarbon-like deposits (C-C and C-H bonds). The survey spectra were taken at the analyzer pass energy of 50 eV and the detailed spectra (valence band + O2s + Ta4f, C1s and O1s) were registered at 20 eV. A Shirley-type background was subtracted from each spectrum. The line shape used for fitting the Ta4f spectra was the product of Lorentzian and Gaussian functions. The concentration ratios of the elements on the sample surface were calculated from the integral photoelectron peak intensities, which were corrected with the theoretical sensitivity factors based on Scofield photoionization cross-sections [25].

Ab initio quantum-chemistry calculations were carried out using an orthorhombic modification of tantalum pentoxide λ-Ta_2O_5. It was used instead of an amorphous material, which is rather challenging in this type of calculation, because its electronic structure was consistent with the electronic structure of the amorphous tantalum oxide [26]. Moreover, it was shown that the electronic structures of oxygen vacancies in amorphous and λ-Ta_2O_5 oxides are similar [27]. The quantum-chemical calculations were made in terms of the density functional theory (DFT) within the periodic supercell model in the Quantum-ESPRESSO code [28]. Hybrid exchange-correlation functional B3LYP was used to reproduce the correct tantalum oxide bandgap of 4.2 eV [29]. The norm-conserving pseudopotentials with the configurations of $5d^3 6\,s^2$ for Ta and $2s^2 2p^4$ for O were used, with a plane-wave cutoff of 950 eV. The atomic ratio [O]/[Ta] was varied by changing the supercell size from which the oxygen atoms were removed. The supercell is constructed by translating the 14-atom unit cell along the crystallographic axes. The valence band (VB) XPS was calculated by summing the projected
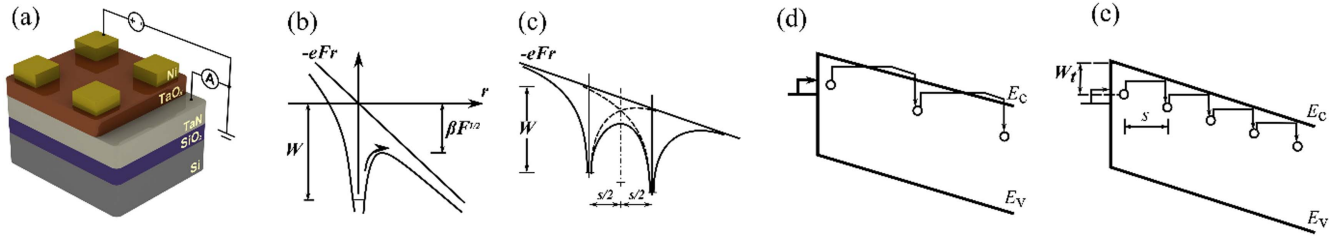
Figure 1. (a) Schematic illustration of the TaN/TaO$_x$/Ni structure used in charge transport measurements. (b) Frenkel model of Coulomb traps ionization in an electric field. (c) Hill model of overlapping Coulomb traps. (d) Makram-Ebeid and Lannoo model of multi-phonon ionization of isolated traps. (e) Nasyrov–Gritsenko model of the phonon-assisted electron tunneling between nearby traps.

densities of states of the valence orbitals taken with the weight factors equal to the corresponding photoionization cross-sections, with Gauss function broadening with the full width at half maximum (FWHM) of 0.6 eV.

The current–voltage characteristics of the MIM samples were measured at temperatures ranging from 20 °C to 80 °C, using a Keithley 6517a electrometer. Serial resistance for TaO$_x$ was measured at a probe station M150 with an Agilent E4980A. During these measurements, short and long corrections as well as cable resistances were taken into account.

To reveal the tantalum oxide conductivity mechanism, we examined the possible charge transport models where the conductivity is limited by traps ionization. We analyzed four models: Frenkel [30, 31], Hill [32, 33], Makram-Ebeid and Lannoo (ME-L) [34], and Nasyrov–Gritsenko [35, 36]. Direct tunneling injection and Fowler–Nordheim mechanisms were not considered since they are temperature-independent. Schottky injection mechanism was also excluded since it is a type of Frenkel model but with an optical dielectric constant ε_∞ four times smaller. We did not consider the trap-assisted tunneling (TAT) of electrons through a traps mechanism as it is suitable for thin films only (with a thickness of less than 10 nm). The space-charge limited current (SCLC) model was omitted because it has a power-law dependence of the current on the voltage and it works only for small barriers at a metal-dielectric interface. Ohm's law cannot explain the exponential dependence of the current on the voltage which we observed for Ta$_2$O$_5$-based structures.

The current density j through the material containing traps can be described by the equation [37, 38]:

$$j = eN^{2/3}P, \qquad (1)$$

where e is the electron charge, N is the trap concentration, and P is the probability of electron emission from traps per second. The Frenkel mechanism is the thermal ionization of an isolated Coulomb trap in an electric field, which involves reducing the energy barrier by applying an electric field (figure 1(b)) [30, 31]:

$$P = \nu \exp\left(-\frac{W - \beta_F \sqrt{F}}{kT}\right), \qquad (2)$$

where W is the trap thermal ionization energy, ν is an attempt-to-escape factor (electron collisions frequency with the walls of the potential well evaluated in the Frenkel model as W/h, where h is the Planck constant), $\beta = \sqrt{e^3/\pi\varepsilon_\infty\varepsilon_0}$ is the Frenkel constant, F is the electric field, k is the Boltzmann constant, T is the

temperature, ε_∞ is the dynamic dielectric permittivity and ε_0 is the dielectric constant.

The Hill model of overlapping Coulomb traps (figure 1(c)) is described by the equation [32, 33]:

$$P = 2\nu \exp\left(-\frac{W - \frac{q^2}{\pi\varepsilon_\infty\varepsilon_0 s}}{kT}\right) \sinh\left(\frac{eFs}{2kT}\right). \qquad (3)$$

Here, $s = N-1/3$ is the distance between traps. According to the ME-L model, the charge transport in a dielectric is governed by multi-phonon ionization of isolated traps (figure 1(d)). The trap ionization probability in that model is described by the equation [34]:

$$P = \sum \exp\left(\frac{nW_{ph}}{2kT} - \frac{W_{opt} - W_t}{W_{ph}} \coth \frac{nW_{ph}}{2kT}\right)$$
$$\times I_n\left(\frac{W_{opt} - W_t}{W_{ph} \sinh(W_{ph}/2kT)}\right) P_i(W_t + nW_{ph}) \qquad (4)$$

$$P_i = \frac{eF}{2\sqrt{2m^*W}} \exp\left(-\frac{4}{3}\frac{\sqrt{2m^*}}{\hbar eF}W^{3/2}\right). \qquad (5)$$

Here, W_t is the thermal trap energy, W_{opt} is the optical trap energy, W_{ph} is the phonon coupled to the defect level energy, and m^* is the electron effective mass.

The Nasyrov–Gritsenko model is the model of phonon-assisted tunneling between traps (PATT). In the PATT model, the act of charge transfer occurs via the electron tunneling between the neighboring traps with multi-phonon excitation (figure 1(e)). In this model, electrons tunnel between the deep traps without excitation in the conduction band, as is the case with Mott hopping. This mechanism was shown to be dominant for high trap densities. In this case, the trap ionization probability is [35, 36]:

$$P = \nu \exp\left(-\frac{W_{opt} - W_t}{2kT}\right) \exp\left(-\frac{2s\sqrt{2m^*W_t}}{\hbar}\right)$$
$$\times \sinh\left(\frac{eFs}{2kT}\right), \qquad (6)$$

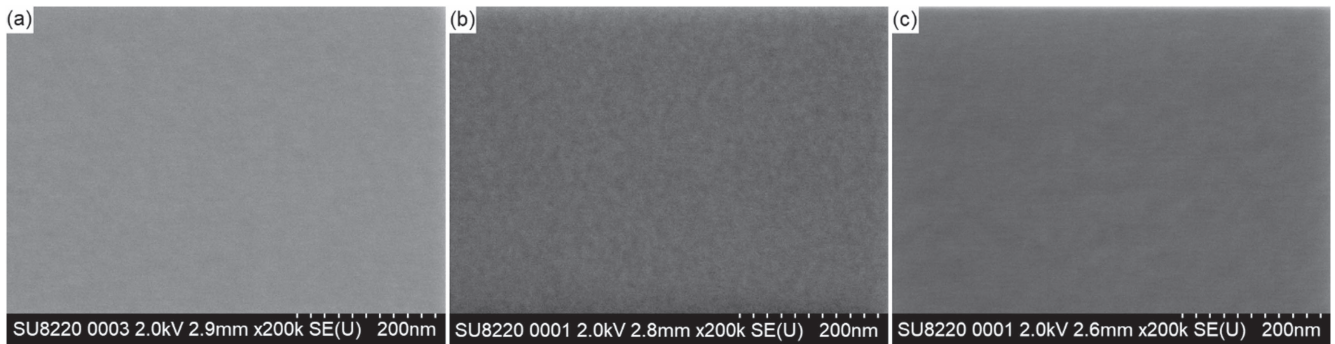$$\nu = \frac{\sqrt{2\pi}\,\hbar W_t}{m^*s^2\sqrt{kT(W_{opt} - W_t)}}. \qquad (7)$$

Figure 2. FESEM images of the TaO$_x$ films grown at different O$_2$ partial pressures: 1.08×10^{-3} Pa (a), 1.35×10^{-3} Pa (b) and 2.21×10^{-3} Pa (c).

The agreement of the theoretical and experimental lg(j)-F curve is set by slope, temperature spread, and absolute values. The temperature spread is determined uniquely (regardless of other parameters) by the trap energy. The slope is also set unambiguously: by ε_∞ for the Frenkel model, by m^* for ME-L and by N for the Hill and Nasyrov–Gritsenko models. Thus, although various models contain 4–5 fitting parameters, firstly, some of them are uniquely determined; secondly, some parameters are interdependent; and thirdly, there is a limited variation range for each parameter.

The trap concentration N range can be estimated using the average distance between the traps s by the formula $N = s^{-3}$. Reasonable values of s range from interatomic distances to dielectric layer thickness d (in our case $d(\max) = 50$ nm). If $s > d$, the probability of at least one defect detection in the film is less than 1 and the current through the MIM structure will be limited by direct tunneling, or injection by Fowler-Nordheim, or injection by Schottky mechanisms. Thus, the possible values of $N \sim 10^{16}$–10^{22} cm^{-3}. The typically reported values of N for Ta$_2$O$_5$ are in the order of 10^{18}–10^{20} cm^{-3} [5, 19, 20, 39, 40]. The expected value for trap energy W for Ta$_2$O$_5$ is about 1 eV, as with other high-κ dielectrics such as HfO$_2$, ZrO$_2$, and Al$_2$O$_3$. The reported W values for Ta$_2$O$_5$ are about 0.7–0.85 eV [18, 20, 23, 41]. W_t is typically the same as W, and W_{opt} is about two times more than W_t. The expected value of ε_∞ for Ta$_2$O$_5$ is 4.4–5.1 and is defined from different optical experiments as $\varepsilon_\infty = n^2$ [42, 43]. The expected m^* value for Ta$_2$O$_5$ is in the range of $(0.3$–$0.7)m_0$ (m_0 is the free electron mass) predicted from the first-principles simulations of various Ta$_2$O$_5$ allotropic modifications [29, 44, 45]. The W_{ph} value is of the order of 10 meV (typically 20–60 meV) and its variation in this range has a negligible effect on the lg(j)-F slope, position and temperature spread of lg(j)-F curves. Finally, the ν parameter is evaluated as W/h and for Ta$_2$O$_5$ it should be of the order of 10^{14}–10^{15} s^{-1}.

3. Results and discussion

Figure 2 shows the FESEM images of the tantalum oxide films grown at different O$_2$ partial pressures. Our earlier investigations of IBSD-deposited HfO$_x$ films [46] using FESEM images and XPS spectra analysis revealed the presence of 10–80 nm metal clusters distributed throughout the film. Unlike in that case, the FESEM images of TaO$_x$ films grown at different O$_2$ partial pressures and presented in figure 2 do not reveal the presence of such clusters. Nonetheless, as shown below, XPS spectra analysis of these films points to the presence of a metallic Ta phase. Hence, we assume that metallic Ta clusters do not appear in the FESEM images of TaO$_x$ films because the resolution at which the images were captured was insufficient for the clusters to be distinguished. In other words, the FESEM images in figure 2 do not exclude the presence of metallic Ta clusters less than 20 nm in size.

The presence of metal tantalum phase in studied TaO$_x$ films is proved by the XPS data of Ta 4f levels in TaO$_x$ with different compositions (figure 3). For the tantalum oxide grown at the highest oxygen pressures, the XPS Ta $4f_{5/2,7/2}$ peak is observed at an energy corresponding to the stoichiometric Ta$_2$O$_5$ and consists of the spin–orbit doublet Ta $4f_{5/2,7/2}$ with the 1.89 eV splitting. Decreasing the oxygen pressure during the tantalum oxide synthesis results in the appearance of new features in the Ta 4f spectra at the lower binding energy side, which corresponds to a partially reduced Ta (suboxides TaO$_y$) and metallic tantalum. The XPS spectra for such a film are well described, with three doublets having Ta $4f_{7/2}$ binding energies of 21.25 eV related to metal Ta, 22.41 eV and 24.54 eV related to TaO$_y$, and 25.95 eV related to Ta$_2$O$_5$. This can be attributed to Ta^{1+}, Ta^{2+}, Ta^{3+}/Ta^{4+}, and Ta^{5+}, respectively [44], and it indicates the presence of oxygen vacancies in the studied films. The atomic ratio [O]/[Ta], as well as the phase composition of TaO$_x$ calculated from the core level XPS data, are presented in table 1.

The dependence of the tantalum coordination number as a function of parameter x was investigated in [47]. It was found that in Ta$_2$O$_5$, the Ta coordination number is 6, which corresponds to the structural unit Ta-O(6). For TaO$_x$, the Ta coordination number decreases to 5 (structural unit Ta-O(5)), as oxygen atomic concentration decreases. The oxide structure in general can be described by the random mixture (RM) or random bonding (RB) model [48]. In the RM model, TaO$_x$ is a mixture of two phases of stoichiometric Ta$_2$O$_5$, consisting of Ta-O(6) structural units and metallic Ta. In the RB model, TaO$_x$ consists of the same structural units Ta-O(6) with the O atoms substitution to the Ta atom: Ta-Ta(ν)O(6-ν), $\nu = 0$, 1, 2, 3, 4, 5, 6. Thus, according to our XPS analysis, the
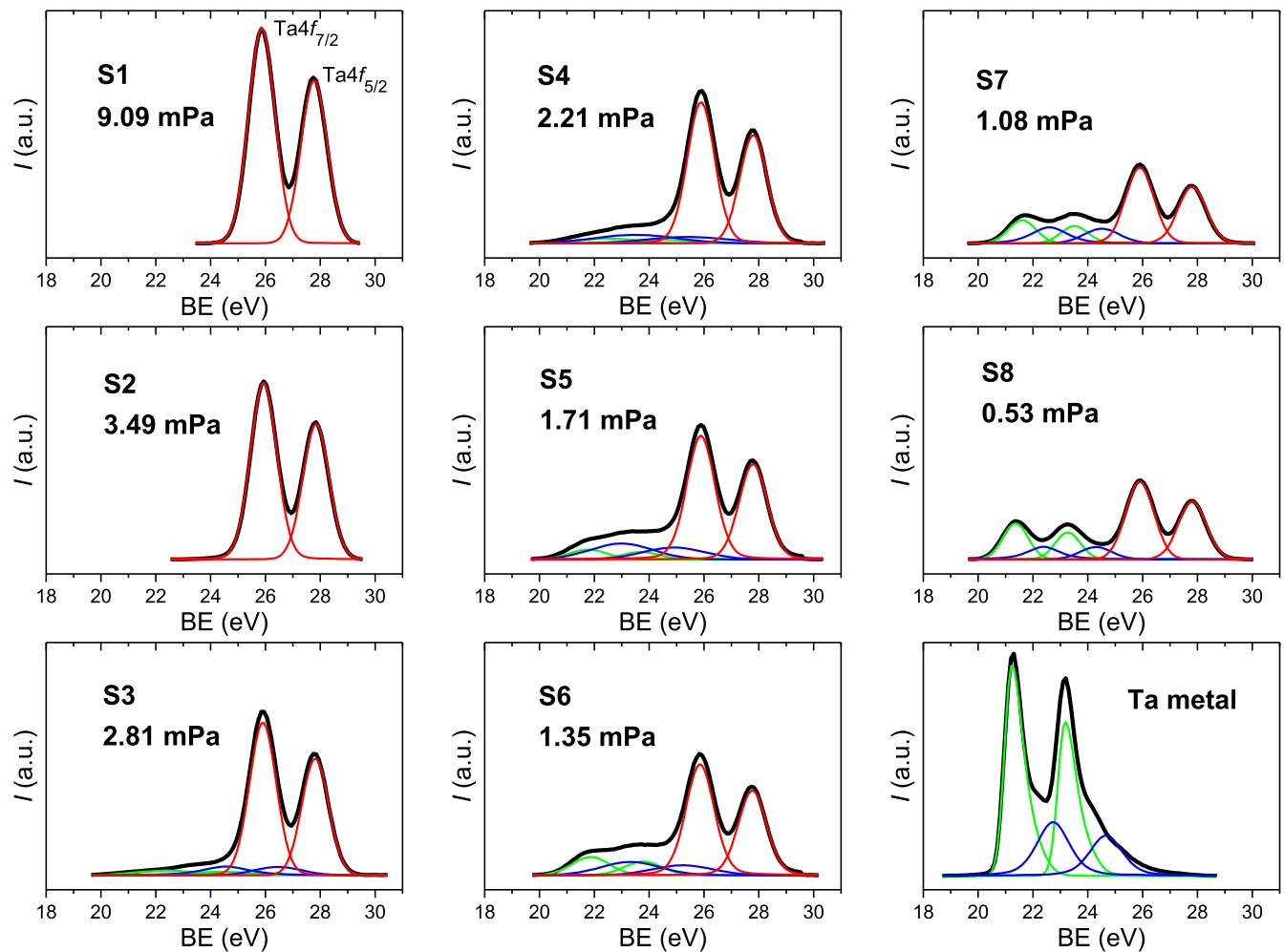
Figure 3. Ta $4f$ photoelectron spectra of eight samples (S1–S8) of tantalum oxide films (black), synthesized under different partial pressures of oxygen in the growth chamber, as well as the XPS spectra of metal tantalum and their deconvolution (colored).

structure of TaO$_x$, enriched with metal, cannot be described either by the RM model or by the RB model.

The Ta $4f$ photoelectron spectra confirm the samples' oxygen depletion, although the numerical accuracy in determining the stoichiometry does not allow for quantitative conclusions, because the accuracy in determining the stoichiometry from the XPS data typically amounts to about 10%. The oxygen depletion increase leads to increasing the photoelectron peak at about 2 eV above the Ta$_2$O$_5$ VB top (figure 4). The experimental VB XPS spectra of all samples are in good agreement with the simulated ones for crystalline Ta$_2$O$_5$ with oxygen vacancies. The calculated bandgap peak in the XPS spectra varies with the proportion to the O vacancies concentration, i.e. by the atomic ratio [O]/[Ta]. Thus, we propose a method for determining the stoichiometry from a comparison of experimental and theoretical VB photoelectron spectra. The atomic ratio [O]/[Ta] in the theoretical model, at which the calculated bandgap peak describes the experimental one, corresponds to the atomic ratio [O]/[Ta] in the studied film. The VB XPS spectra for S1 are described by the theoretical spectra for perfect Ta$_2$O$_5$; S2, for the Ta$_2$O$_5$ 168-at. cell with one oxygen vacancy V$_O$; S3, for the Ta$_2$O$_5$ 42-at. cell with one V$_O$; S4, for the Ta$_2$O$_5$ 56-at. cell with

three V$_O$; S5, for the Ta$_2$O$_5$ 56-at. cell with five V$_O$; S6, for the Ta$_2$O$_5$ 42-at. cell with three V$_O$; S7, for the Ta$_2$O$_5$ 28-at. cell with two V$_O$, and S8, for the Ta$_2$O$_5$ 28-at. cell with five V$_O$.

One can see in table 1 that the atomic ratio [O]/[Ta] defined from the integral photoelectron peak intensities of core levels corelates with the [O]/[Ta] ratio defined from the comparison of experimental and theoretical VB XPS. At the same time, it can be expected that the method of determining the [O]/[Ta] atomic ratio in the frame of the DFT simulation has a higher numerical accuracy. Thus, we can determine the value of x for the TaO$_x$ films used in the transport measurements by knowing the dependence of the atomic ratio [O]/[Ta] on the O$_2$ partial pressure in the IBSD growth chamber (table 1). For the films synthesized at $P(O_2)$ at 9.34, 6.05, 3.91, 3.27 and 2.66 mPa, the [O]/[Ta] ratios should be 2.5, 2.49, 2.48, 2.47 and 2.4, respectively.

It was found that the experimental current–field (j–F) characteristics of the TiN/Ta$_2$O$_5$/Ni structure, measured at different temperatures, can be formally described by the Frenkel, Hill, ME-L and Nasyrov–Gritsenko models (figure 5). At $j = 10^{-8}$–10^{-7} A cm^{-2} and a contact area of $100 \times 100\,\mu$m, the current magnitude is 0.1–1 nA. So, the
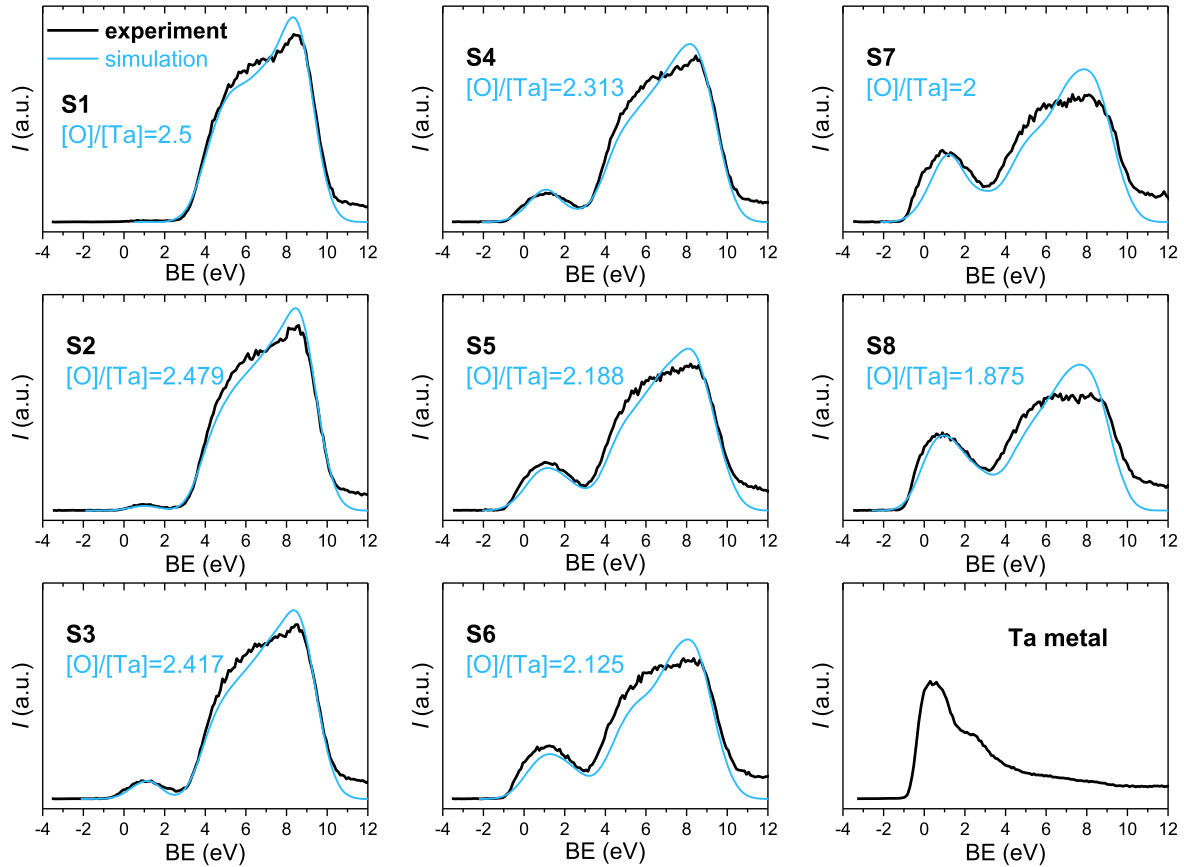
Figure 4. VB XPS of eight samples of tantalum oxide films synthesized at different O_2 pressures in a growth chamber (black), in comparison with the calculated ones (blue) for λ-Ta_2O_5 with different atomic ratios [O]/[Ta]. S1: perfect crystal. S2: one V_O in 168 atoms. S3: one V_O in 42 atoms. S4: three V_O in 56 atoms. S5: five V_O in 56 atoms. S6: three V_O in 42 atoms. S7: two V_O in 28 atoms. S8: five V_O in a supercell of 28 atoms.
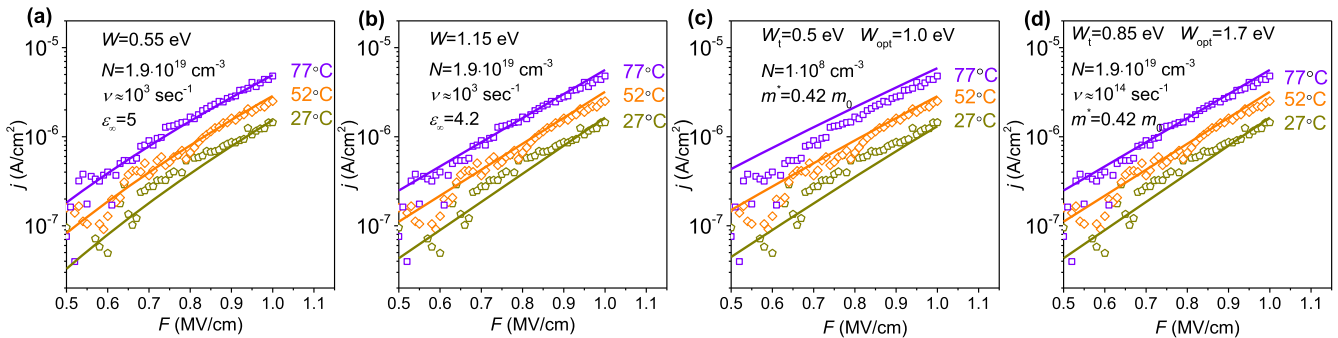

Figure 5. Experimental (symbols) and simulated (solid) j–F characteristics of Ta_2O_5 at different temperatures. The simulated curves are in the Frenkel model (a), Hill model (b), ME-L model (c) and PATT model (d). The parameters used for fitting in all models are presented in the graphs.

noise at low current becomes comparable to the current value itself at a semilog scale. The noise at high electric field ($> 0.7\,\mathrm{MV\,cm^{-1}}$) is small enough to observe a shift to a higher current density region with the increase in temperatures. In turn, it is the lg(j)-F curves spread over the temperatures that allows the determining of the trap energy values. The sensitivity of the spread value to the trap energy parameters is high for all models due to the exponential dependence. The accuracies of determining W and ($W_{opt}-W_t$) are less than 3%–5%.

Fitting by the Frenkel model allows us to obtain the reasonable physical values of $N = 1.9 \cdot 10^{19}\,\mathrm{cm^{-3}}$, $W = 0.55\,\mathrm{eV}$, and $\varepsilon_\infty = 5$. However, the attempt-to-escape frequency value necessary for fitting $\nu = 10^3\,\mathrm{s^{-1}}$ is many orders of magnitude lower than the characteristic value $\nu \sim W/h = 1.3 \cdot 10^{14}\,\mathrm{s^{-1}}$. With $\nu = 1.3\ 10^{14}\,\mathrm{s^{-1}}$ the trap concentration should be $4 \cdot 10^7\,\mathrm{cm^{-3}}$. The anomalously small traps concentration indicate that the Frenkel effect does not describe the charge transport in Ta_2O_5. Similarly, the Hill model of overlapping Coulomb traps is not suitable to
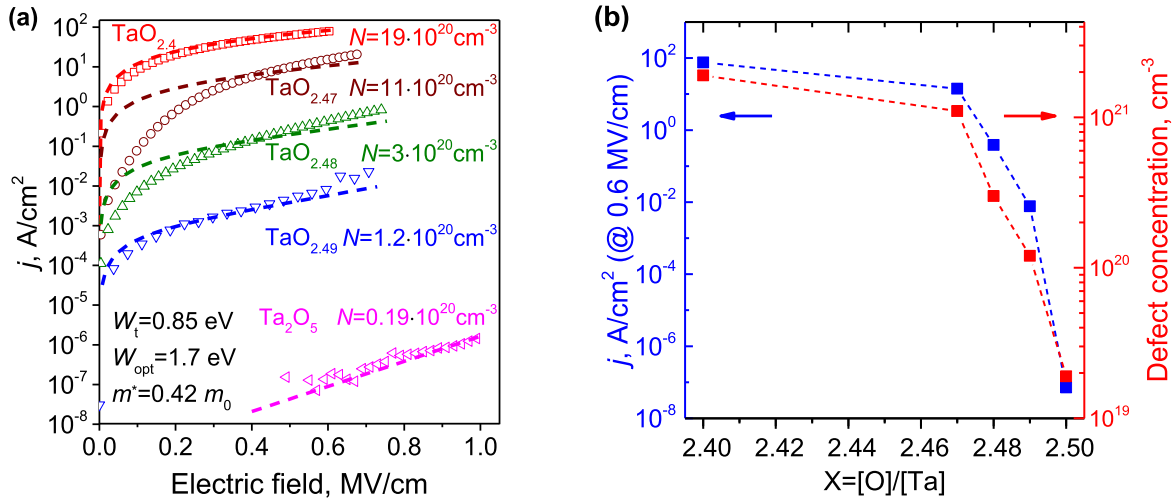
Figure 6. (a) Experimental (symbols) and simulated in frame of PATT model (dashed lines) j–F characteristics of TaO$_x$ of different composition at room temperature. The parameters used for fitting are presented in the graphs. (b) The dependence of the current *j* and defects concentration *N* on *x* at a fixed field of 0.6 MV cm^{-1}.

describe the transport in Ta$_2$O$_5$. The agreement of calculation and experiment in this case is achieved with the reasonable values of $N = 1.9 \cdot 10^{19}$ cm^{-3}, $W = 1.15$ eV and $\varepsilon_\infty = 4.2$. However, the fitting of the attempt-to-escape frequency value is 10^3 s^{-1}.

The ME-L model of multi-phonon ionization of isolated traps can be used to qualitatively describe the Ta$_2$O$_5$ conductivity only in strong fields. In this case, the agreement of calculation and experiment is achieved at reasonable values of $W_t = 0.5$ eV, $W_{opt} = 1.0$ eV, $W_{ph} = 60$ meV and $m^* = 0.42$ m_0, but with an unacceptably low traps concentration of $N = 1 \cdot 10^8$ cm^{-3}. That concentration corresponds to the distance between the traps ~ 2 μm, which is much larger than the film thickness. It is concluded that the ME-L model is also not suitable to describe the Ta$_2$O$_5$ conductivity.

The Nasyrov–Gritsenko PATT model adequately represents the experimental j–F characteristics, both qualitatively and numerically. The fitting parameters $\nu \approx 10^{14}$ s^{-1}, $N = 1.9 \cdot 10^{19}$ cm^{-3}, $W_t = 0.85$ eV, $W_{opt} = 1.7$ eV, and $m^* = 0.42$ m_e have clear physical meanings. The $W_t = 0.85$ eV value is in good agreement with the reported trap energies in Ta$_2$O$_5$: 0.8 eV [18, 41], 0.85 eV [20] and 0.7 eV [23]. The m^* fits the theoretical range of $(0.3–0.7)m_0$ [29, 44, 45]. The $W_{opt} = 1.7$ eV value is close to the optical trap energy of 1.5 eV extracted from the photoconductivity experiments [49]. It turns out that, for tantalum oxide, the optical trap energy is equal to two thermal trap energy values, as was earlier observed in Al$_2$O$_3$ [50], HfO$_2$ [51], and Hf$_{0.5}$Zr$_{0.5}$0$_2$ [52].

The j–F curves of five TaO$_x$ samples with different [O]/[Ta] atomic ratios are also well described by the PATT model, with the same values of W_t, W_{opt} and m^* (figure 6(a)). The decrease of *x* leads to the eight orders of magnitude increase in current density at 0.4 MV cm^{-1}. The simulation within the PATT model shows that this effect can be explained by the trap density increase in the TaO$_x$ films from $1.9 \cdot 10^{19}$ cm^{-3} for (almost) stoichiometric Ta$_2$O$_5$, to $1.9 \cdot 10^{21}$ cm^{-3} for TaO$_{2.42}$. The calculated and experimental lg(*j*)–F curves diverge at small electric fields for two reasons.

Firstly, the current is limited by the charges contact injection from electrodes into traps in the dielectric. Secondly, the PATT model is based on stationary currents and does not consider the current relaxation due to carriers trapping in a dielectric, which can have a significant impact on current–field curves at low electric fields [39]. Therefore, the low-fields part of the model does not necessarily describe the experiment. We cannot state unequivocally why, for samples with $x = 2.47$ and 2.48, the conformity of calculation and experiment at the low field region is worse than for the samples with $x = 2.4$ and 2.49. We draw our conclusions based on the correspondence of simulation and experiment at high electric fields. The *F* ranges in the lg(*j*)–F curves for Ta$_2$O$_5$ and TaO$_x$ differ because the higher current is limited by the TaO$_x$ film breakdown field, while the low current in stoichiometric Ta$_2$O$_5$ is limited by the sensitivity of our experimental equipment.

The dependence of the current density *j* on *x* at the fixed field is similar to the dependence of the theoretical defects concentration *N* on *x* (figure 6(b)), and the graphics for various fixed fields coincide. This fact is an argument in favor of the fairness of the PATT model in explaining leakage current dependence on the traps concentration in TaO$_x$. The dependences *j*/(N) versus *x* are significantly stronger for a weak oxygen depletion in TaO$_x$ than for highly oxygen-depleted TaO$_x$. This is a qualitatively expected result: when the *x* value decreases, the contribution of metallic conductivity of TaO$_x$ increases.

Thus, we show the direct dependence of the current density through the TaO$_x$ film on its atomic radion [O]/[Ta]. Oxygen vacancies acting as traps permit explanation of the low resistance values for SET and the RESET states for TaO$_x$ ReRAM [53–56]. In these memories, the typical values of SET resistance are 6–8 kΩ, while the RESET values are of the order of 200 kΩ to 300 kΩ. For the discussed TaOx film with the minimal value of *x* (figure 6(a)) and for the readout field ~ 1 MV cm^{-1}, the current densities are of the order of 10^2 A cm^{-2}. For a memory cell of ~ 1 μm^2 area, this

corresponds to a resistance $\sim 1\,\text{M}\Omega$. The low SET resistance after the forming suggests that oxygen vacancies concentration much higher than $2 \cdot 10^{20}\,\text{cm}^{-3}$ exists both in the stoichiometric and nonstoichiometric tantalum oxide films of the ReRAM device. Such a filament can be modeled as a percolation path comprising TaO_x with a very high oxygen vacancies concentration (much higher than for $x = 2.4$). The maximum vacancies concentration in this work ($\sim 2 \cdot 10^{20}\,\text{cm}^{-3}$) is far from the percolation threshold of oxygen vacancies ($\sim 1.7 \cdot 10^{22}\,\text{cm}^{-3}$ evaluated from the typical value of metal percolation limit: $\sim 40\%$ of metal). The oxygen deficiency at the level necessary for a percolation (spanning of vacancies from one side of the TaO_x film to the other) is not practical for device fabrication. Thus, the presented results suggest that oxygen vacancies with a concentration close to the percolation threshold are created both in the TaO_x and Ta_2O_5 layers of the stacked device during the forming process. The electrical current is carried by hopping the electrons between the Ta ions separating the vacancies.

4. Conclusion

The electronic structure and charge transport of tantalum oxide films with different [O]/[Ta] atomic ratios were investigated experimentally and in the frames of *ab initio* simulation. According to photoelectron spectroscopy, TaO_x consists of Ta_2O_5, metallic tantalum clusters and tantalum suboxides TaO_y. The electron microscopy data showed that the diameter of the metallic Ta clusters does not exceed 20 nm. A method for evaluating the atomic ratio [O]/[Ta] in TaO_x from a comparison of experimental and theoretical valence band photoelectron spectra is proposed. Current–field characteristics of Ta_2O_5 at different temperatures have been experimentally studied. The current-field characteristics of Ta_2O_5 at different temperatures were analyzed based on four transport models: Frenkel, Hill, Makram–Ebeid–Lannoo and Nasyrov–Gritsenko. It was shown that the charge transport in stoichiometric and oxygen-deficient tantalum oxide can be consistently described by the Nasyrov–Gritsenko model of phonon-assisted tunneling between traps. The thermal trap energy of 0.85 eV and optical trap energy of 1.7 eV were established. The exponential increase of the leakage current in TaO_x with decreasing x is explained by the increasing oxygen vacancy concentration corresponding to the smaller distance between traps.

Acknowledgments

ORCID iDs

T V Perevalov ⬤ https://orcid.org/0000-0003-0895-6202
V A Gritsenko ⬤ https://orcid.org/0000-0003-1646-0848
A A Gismatulin ⬤ https://orcid.org/0000-0003-3177-6226
V A Voronkovskii ⬤ https://orcid.org/0000-0001-5139-4394
A K Gerasimova ⬤ https://orcid.org/0000-0003-2932-8424
V Sh Aliev ⬤ https://orcid.org/0000-0002-4266-971X
I A Prosvirin ⬤ https://orcid.org/0000-0002-0351-5128

References

[1] Wilk G D, Wallace R M and Anthony J M 2001 High-κ gate dielectrics: current status and materials properties considerations *J. Appl. Phys.* **89** 5243–75
[2] Robertson J 2004 High dielectric constant oxides *Eur. Phys. J. Appl. Phys.* **28** 265–91
[3] Perevalov T V and Gritsenko V A 2010 Application and electronic structure of high-permittivity dielectrics *Phys.-Usp.* **53** 561–75
[4] Robertson J and Wallace R M 2015 High-K materials and metal gates for CMOS applications *Mater. Sci. Eng.* R **88** 1–41
[5] Zhu H, Bonevich J E, Li H T, Richter C A, Yuan H, Kirillov O and Li Q L 2014 Discrete charge states in nanowire flash memory with multiple Ta_2O_5 charge-trapping stacks *Appl. Phys. Lett.* **104** 233504
[6] Lee M J *et al* 2011 A fast, high-endurance and scalable non-volatile memory device made from asymmetric Ta_2O_{5-x}/TaO_{2-x} bilayer structures *Nat. Mater.* **10** 625–30
[7] Prakash A, Jana D and Maikap S 2013 TaO_x-based resistive switching memories: prospective and challenges *Nanoscale Res. Lett.* **8** 418
[8] Wedig A *et al* 2016 Nanoscale cation motion in TaO_x, HfO_x and TiO_x memristive systems *Nat. Nanotechnol.* **11** 67–75
[9] Tsuruoka T, Valov I, Tappertzhofen S, van den Hurk J, Hasegawa T, Waser R and Aono M 2015 Redox reactions at $Cu,Ag/Ta_2O_5$ interfaces and the effects of Ta_2O_5 film density on the forming process in atomic switch structures *Adv. Funct. Mater.* **25** 6374–81
[10] Kim K M, Lee S R, Kim S, Chang M and Hwang C S 2015 Self-limited switching in Ta_2O_5/TaO_x memristors exhibiting uniform multilevel changes in resistance *Adv. Funct. Mater.* **25** 1527–34
[11] Park G S *et al* 2013 *In situ* observation of filamentary conducting channels in an asymmetric Ta_2O_{5-x}/TaO_{2-x} bilayer structure *Nat. Commun.* **4** 2382
[12] Rahaman S Z, Maikap S, Tien T C, Lee H Y, Chen W S, Chen F T, Kao M J and Tsai M J 2012 Excellent resistive memory characteristics and switching mechanism using a Ti nanolayer at the Cu/TaO_x interface *Nanoscale Res. Lett.* **7** 345
[13] Goux L, Fantini A, Chen Y Y, Redolfi A, Degraeve R and Jurczak M 2014 Evidences of electrode-controlled retention properties in Ta_2O_5-based resistive-switching memory cells *ECS Solid State Lett.* **3** Q79–81
[14] Torrezan A C, Strachan J P, Medeiros-Ribeiro G and Williams R S 2011 Sub-nanosecond switching of a tantalum oxide memristor *Nanotechnology* **22** 485203
[15] Nasyrov K A and Gritsenko V A 2013 Transport mechanisms of electrons and holes in dielectric films *Phys.-Usp.* **56** 999–1012
[16] Graves C E, Davila N, Merced-Grafals E J, Lam S T, Strachan J P and Williams R S 2017 Temperature and field-dependent transport measurements in continuously tunable tantalum oxide memristors expose the dominant state variable *Appl. Phys. Lett.* **110** 123501

[17] Yang M K, Ju H, Kim G H, Lee J K and Ryu H C 2015 Direct evidence on Ta-metal phases igniting resistive switching in TaO$_x$ thin film *Sci. Rep.* **5** 14053

[18] Egorov K V, Kuzmichev D S, Chizhov P S, Lebedinskii Y Y, Hwang C S and Markeev A M 2017 *In situ* control of oxygen vacancies in TaO$_x$ thin films via plasma-enhanced atomic layer deposition for resistive switching memory applications *ACS Appl. Mater. Interfaces* **9** 13286–92

[19] Novkovski N and Atanassova E 2005 Origin of the stress-induced leakage currents in Al-Ta$_2$O$_5$/SiO$_2$-Si structures *Appl. Phys. Lett.* **86** 152104

[20] Houssa M, Degraeve R, Mertens P W, Heyns M M, Jeon J S, Halliyal A and Ogle B 1999 Electrical properties of thin SiON/Ta$_2$O$_5$ gate dielectric stacks *J. Appl. Phys.* **86** 6462–7

[21] Vishnyakov A V, Novikov Y N, Gritsenko V A and Nasyrov K A 2009 The charge transport mechanism in silicon nitride: multiphonon trap ionization *Solid-State Electron.* **53** 251–5

[22] Gritsenko V A, Perevalov T V and Islamov D R 2016 Electronic properties of hafnium oxide: a contribution from defects and traps *Phys. Rep.* **613** 1–20

[23] Houssa M, Tuominen M, Naili M, Afanas'ev V V, Stesmans A, Haukka S and Heyns M M 2000 Trap-assisted tunneling in high permittivity gate dielectric stacks *J. Appl. Phys.* **87** 8615–20

[24] Gritsenko V A, Perevalov T V, Voronkovskii V A, Gismatulin A A, Kruchinin V N, Aliev V S, Pustovarov V A, Prosvirin I P and Roizin Y 2018 Charge transport and the nature of traps in oxygen deficient tantalum oxide *ACS Appl. Mater. Interfaces* **10** 3769–75

[25] Scofield J H 1976 Hartree-Slater subshell photoionization cross-sections at 1254 and 1487 eV *J. Electron Spectrosc. Relat. Phenom.* **8** 129–37

[26] Lee S H, Kim J, Kim S J, Kim S and Park G S 2013 Hidden structural order in orthorhombic Ta$_2$O$_5$ *Phys. Rev. Lett.* **110** 235502

[27] Guo Y Z and Robertson J 2015 Comparison of oxygen vacancy defects in crystalline and amorphous Ta$_2$O$_5$ *Microelectron. Eng.* **147** 254–9

[28] Giannozzi P *et al* 2009 QUANTUM ESPRESSO: a modular and open-source software project for quantum simulations of materials *J. Phys.: Condens. Matter.* **21** 395502

[29] Shvets V A, Aliev V S, Gritsenko D V, Shaimeev S S, Fedosenko E V, Rykhlitski S V, Atuchin V V, Gritsenko V A, Tapilin V M and Wong H 2008 Electronic structure and charge transport properties of amorphous Ta$_2$O$_5$ films *J. Non-Cryst. Solids* **354** 3025–33

[30] Frenkel J 1938 On pre-breakdown phenomena in insulators and electronic semi-conductors *Phys. Rev.* **54** 647

[31] Hill R M 1971 Poole-Frenkel conduction in amorphous solids *The Philosophical Magazine* **23** 39

[32] Hill R M 1971 Poole-Frenkel conduction in amorphous solids *The Philosophical Magazine* **23** 59–86

[33] Adachi H, Shibata Y and Ono S 1971 On electronic conduction through evaporated silicon oxide films *J. Phys. D: Appl. Phys.* **4** 988–94

[34] Makram-Ebeid S S and Lannoo M 1982 Quantum model for phonon-assisted tunnel ionization of deep levels in a semiconductor *Phys. Rev.* B **25** 6406

[35] Nasyrov K A and Gritsenko V A 2011 Charge transport in dielectrics via tunneling between traps *J. Appl. Phys.* **109** 093705

[36] Nasyrov K A and Gritsenko V A 2011 Charge transport in dielectrics by tunneling between traps *J. Exp. Theor. Phys.* **112** 1026–34

[37] Sze S M 1981 *Physics of Semiconductor Devices* (New York: Wiley)

[38] Islamov D R, Gritsenko V A and Chin A 2017 Charge transport in thin hafnium and zirconium oxide films *Optoelectron. Instrum.* **53** 184–9

[39] Huang S H 2013 Oxygen annealing effects on transport and charging characteristics of Al-Ta$_2$O$_5$/SiOxNy-Si *IEEE Trans. Electron Devices* **60** 2741–6

[40] Fleming R M, Lang D V, Jones C D W, Steigerwald M L, Murphy D W, Alers G B, Wong Y H, van Dover R B, Kwo J R and Sergent A M 2000 Defect dominated charge transport in amorphous Ta$_2$O$_5$ thin films *J. Appl. Phys.* **88** 850–62

[41] Lau W S, Leong L L, Han T J and Sandler N P 2003 Detection of oxygen vacancy defect states in capacitors with ultrathin Ta$_2$O$_5$ films by zero-bias thermally stimulated current spectroscopy *Appl. Phys. Lett.* **83** 2835–7

[42] Bright T J, Watjen J I, Zhang Z M, Muratore C, Voevodin A A, Koukis D I, Tanner D B and Arenas D J 2013 Infrared optical properties of amorphous and nanocrystalline Ta$_2$O$_5$ thin films *J. Appl. Phys.* **114** 083515

[43] Chaneliere C, Four S, Autran J L, Devine R A B and Sandler N P 1998 Properties of amorphous and crystalline Ta$_2$O$_5$ thin films deposited on Si from a Ta(OC$_2$H$_5$)$_5$ precursor *J. Appl. Phys.* **83** 4823–9

[44] Ivanov M V, Perevalov T V, Aliev V S, Gritsenko V A and Kaichev V V 2011 Electronic structure of d-Ta$_2$O$_5$ with oxygen vacancy: *ab initio* calculations and comparison with experiment *J. Appl. Phys.* **110** 024115

[45] Perevalov T V and Shaposhnikov A V 2013 *Ab initio* simulation of the electronic structure of Ta$_2$O$_5$ crystal modifications *J. Exp. Theor. Phys.* **116** 995–1001

[46] Aliev V S, Gerasimova A K, Kruchinin V N, Gritsenko V A, Prosvirin I P and Badmaeva I A 2016 The atomic structure and chemical composition of HfOx (x < 2) films prepared by ion-beam sputtering deposition *Mater. Res. Express* **3** 085008

[47] Tsuchiya T, Imai H, Miyoshi S, Glans P A, Guo J H and Yamaguchi S 2011 X-Ray absorption, photoemission spectroscopy, and Raman scattering analysis of amorphous tantalum oxide with a large extent of oxygen nonstoichiometry *Phys. Chem. Chem. Phys.* **13** 17013–8

[48] Gritsenko V A 2008 Atomic structure of the amorphous nonstoichiometric silicon oxides and nitrides *Phys.-Usp.* **51** 699–708

[49] Thomas J H 1973 Defect photoconductivity of anodic Ta$_2$O$_5$ films *Appl. Phys. Lett.* **22** 406–8

[50] Novikov Y N, Gritsenko V A and Nasyrov K A 2009 Charge transport mechanism in amorphous alumina *Appl. Phys. Lett.* **94** 222904

[51] Gritsenko V A, Islamov D R, Perevalov T V, Aliev V S, Yelisseyev A P, Lomonova E E, Pustovarov V A and Chin A 2016 Oxygen vacancy in hafnia as a blue luminescence center and a trap of charge carriers *J. Phys. Chem. C* **120** 19980–6

[52] Islamov D R, Perevalov T V, Gritsenko V A, Cheng C H and Chin A 2015 Charge transport in amorphous Hf$_{0.5}$Zr$_{0.5}$O$_2$ *Appl. Phys. Lett.* **106** 102906

[53] Panasonic Starts World's First Mass Production of ReRAM Mounted Microcomputers, in, (http://news.panasonic.com/global/press/data/2013/07/en130730-2/en130730-2.html), 2013

[54] Ninomiya T, Arita K, Mikawa T and Fujii S 2013 Nonvolatile memory element and method for manufacturing the same *US Patent Specification* US8441060B2

[55] Wei Z Q, Ninomiya T, Muraoka S, Katayama K, Yasuhara R and Mikawa T 2014 Switching and reliability mechanisms for ReRAM *2014 IEEE Int. Interconnect Technology Conf./Advanced Metallization Conference (IITC/AMC)* pp 349–51

[56] Kim B Y, Lee K J, Chung S O, Kim S G, Ko Y S and Kim H S 2016 Low power switching of Si-doped Ta$_2$O$_5$ resistive random access memory for high density memory application *Jpn. J. Appl. Phys.* **55** 04EE09